THE ASTRONOMICAL JOURNAL VOLUME 114, NUMBER 6 DECEMBER 1997

NUCLEAR ROTATION CURVES OF GALAXIES IN THE CO-LINE EMISSION

YOSHIAKI SOFUE, YOSHINORI TUTUI, MAREKI HONMA, AND AKIHIKO TOMITA
Institute of Astronomy, University of Tokyo, 2-21-1 Osawa, Mitaka, Tokyo 181, Japan
Electronic mail: sofue@mtk.ioa.s.u-tokyo.ac.jp

Received 1997 May 16; accepted 1997 August 27

ABSTRACT

We have obtained high-resolution position-velocity (PV) diagrams along the major axes of the central regions of nearby galaxies in the CO-line emission using the Nobeyama 45 m telescope and the Millimeter Array. Nuclear rotation curves for 14 galaxies have been derived based on the PV diagrams using the envelope-tracing method. The nuclear rotation curves for most of the galaxies show a steep rise within a few hundred pc, which indicates a high-density concentration of mass. © *1997 American Astronomical Society.* [S0004-6256(97)02512-0]

1. INTRODUCTION

Rotation curves (RC) of galaxies have been supposed to generally show a rigid-body rise in the central few kpc region, followed by a flat rotation in the disk and outer regions (Rubin *et al.* 1980, 1982; Mathewson *et al.* 1996; Persic *et al.* 1995). Although the H I rotation curves are most useful for investigating the dark halo and total mass for its extended distribution in the outer region (e.g., Kent 1987), the H I gas is deficient in the central regions. Therefore, H I rotation curves may be not accurate enough to discuss the nuclear rotation. The current optical rotation curves, which were obtained primarily for the study of dark halo in the outermost regions, had been overexposed in the central regions, and may not indicate the true nuclear rotation within the bulges.

It is well known that the detailed rotation curve for our Milky Way Galaxy shows a very steep rise in the central few hundred pc (e.g., Clemens 1985). A simple question arises, if the true rotation curves of galaxies, particularly for the innermost regions, would be more like that for our Galaxy. In order to clarify this question, we have proposed to use the CO-line data for the central regions, where the molecular gas dominates over the H I gas (Sofue *et al.* 1994; Honma *et al.* 1995). We have recently used CO-line data for the central parts of nearby galaxies, and obtained combined rotation curves with the outer H I and optical curves (Sofue 1996, 1997: Paper I and II). We have shown that the nuclear CO rotation curves generally rise sharply in the central few hundred parsecs than those derived from H I and optical observations alone. More recently, Rubin *et al.* (1997) have also shown that the central rotation curves rise steeply within a few hundred pc, indicating a massive rotating disk around the nucleus, from their Hα spectroscopy of Virgo-cluster spirals.

In this paper, we present the result of high-resolution CO-line observations along the major axes of the central regions of nearby galaxies using the Nobeyama 45 m telescope and the NMA (Nobeyama Millimeter Array). We aim to provide basic data for the study of nuclear rotation curves, as well as to clarify whether the nuclear steep rise is indeed a universal characteristics for spiral galaxies.

2. OBSERVATIONS

2.1 Observations with the 45-m Telescope

Observations of the CO ($J=1-0$) line with the 45 m telescope were made on 1996 March 16–20 (NGC 2903, 3521, 4631, 5055, 7331), and December 18–20 (NGC 598, 1003, 2403, 3198, 3953, 4096, 5457 (M101), 6674, and UGC 2855). The antenna had a HPBW of 15″ at the CO-line frequency, and the aperture and main-beam efficiencies were $\eta_a=0.35$ and $\eta_{\rm mb}=0.50$, respectively. We used two SIS (superconductor-insulator-superconductor) receivers with orthogonal polarization, which were combined with 2048-channel acousto-optical spectrometers. The total channel number corresponds to a frequency width of 250 MHz, and, therefore, to a velocity coverage in the rest frame at the galaxy of 650 km s^{-1} with a resolution of 650/2048 km s^{-1}. The center frequency was tuned to coincide with the systemic velocity of the galaxies.

We scanned the major axis of each galaxy at a spacing of 7.″5 for the central ±30″ region, and at 15″ for the outer regions. After combining every 32 channels in order to increase the signal-to-noise ratio, we obtained spectra with a velocity resolution of 10.2 km s^{-1}. The calibration of the line intensity was made using an absorbing chopper in front of the receiver, yielding an antenna temperature (T_A^*), corrected for both the atmospheric and antenna ohmic losses. We used a multiple-on and off switching mode, and the on-source total integration time per data point was typically fifteen minutes. The system noise temperature (SSB) was 500–800 K. After flagging and subtraction of baselines, the spectra were smoothed to a velocity resolution of 10 km s^{-1} (32 channels). The rms noise of the resultant spectra at a velocity resolution of 10 km s^{-1} was typically 20 mK in T_A^*. The pointing of the antenna was corrected and checked by observing nearby SiO maser sources at 43 GHz every 1 to 1.5 hours, and the error was typically within ±3″.

 0004-6256/97/114(6)/2428/9/$10.00

TABLE 1. Parameters for the observed galaxies.

Galaxy	Type	RA_{1950} (h m s)	$Decl_{1950}$ (° ′ ″)	$V_{sys,(hel\ or\ lsr)}$ (km/s)	Tele/BW (″)	Obs. Date
NGC 598	Sc	01 31 01.67	30 24 15.0	-175(hel)	45m/15	Dec-1996
NGC 1003	Scd	02 36 06.12	40 39 28.0	620(hel)	45m/15	Dec-1996
NGC 2403	Sc	07 32 05.50	65 42 40.0	100(lsr)	45m/15	Dec-1996
UGC 2855	SBc	03 43 15.70	69 58 46.0	1200(hel)	45m/15	Dec-1996
NGC 2903	Sc	09 29 20.30	21 43 23.9	550(lsr)	45m/15	Mar-1996
NGC 3034	Ir	09 51 43.48	69 55 00.8	200(lsr)	45m/15	Dec-1996
NGC 3198	SBc	10 16 51.94	45 48 06.0	665(lsr)	45m/15	Dec-1996
NGC 3521	Sbc	11 03 15.10	00 13 58.0	800(lsr)	45m/15	Mar-1996
NGC 4096	Sc	12 03 28.48	47 45 20.0	565(hel)	45m/15	Dec-1996
NGC 4303	Sc	12 19 21.40	04 44 58.0	1560(hel)	NMA/9.2×5.7$_{PA=-14°\ 9}$,	Dec-1994
NGC 4569	Sab	13 26 18.00	12 34 18.7	240(hel)	NMA/9.9×4.8$_{PA=161°\ 8}$,	Dec-1994
NGC 4631	ScIr	12 39 39.70	32 48 48.0	600(lsr)	45m/15	Dec-1992
NGC 5055	Sbc	13 13 34.90	42 17 34.0	555(lsr)	45m/15	Mar-1996
NGC 5457	Sc	14 01 26.31	54 35 17.9	240(hel)	45m/15	Dec-1996
NGC 6674	SBb	18 36 31.00	25 19 55.0	340(hel)	45m/15	Dec-1996
NGC 7331	Sbc	22 34 46.66	34 09 20.9	825(lsr)	45m/15	Mar-1996

2.2 Observations with the Nobeyama Millimeter Array

High-resolution interferometer observations were obtained by using the Nobeyama Millimeter Array (NMA) in the *C* configuration on 1994 December 1–3 (NGC 4501, NGC 4527, NGC 4303), December 15–17 (NGC 4569), and in the *D* configuration on 1995 March 15–17, and March 29–31. In this paper we present the results for NGC 4303 and NGC 4569, for which good PV diagrams have been obtained. The flux and phase calibrations were done by observing the nearby radio source 3C 273, which had a flux density of 22 Jy at the observing frequency. A 1024-channel FX system (a fast-Fourier-transform spectrocorrelator) was used for the spectroscopic data acquisition with a total bandwidth of 320 MHz (831 km s^{-1}). The data were then averaged in 16 bins of original frequency channels resulting in 64 channels with a frequency (velocity) resolution of 5 MHz (13.0 km s^{-1}). The cleaned maps were then combined into a cube of intensity data in the (RA, Dec, V_{LSR}) space. Using these data cube, we obtained position-velocity diagrams along a constant declination across the nucleus for NGC 4303, approximately parallel to the major axis (PA 105°), and along a constant RA for NGC 4569 (major axis at PA 23°).

2.3 Selection of Objects

Observed positions and systemic velocities of the program galaxies are listed in Table 1. Table 2 list the adopted parameters for these galaxies. The galaxies were so chosen that (a) the angular size is large enough in order to obtain a sufficiently high linear-scale resolution in the central regions; (b) the disk is mildly tilted in order for an accurate correction for the inclination to derive the rotation velocity; (c) no high-sensitivity data have been obtained yet with the 45 m telescope or the NMA; and (d) the CO-line emission is sufficiently strong or *IRAS* 60 and 100 μm fluxes are higher than several Jy. For the selection of objects, we have referred to the published CO data from the Five College 14 m telescope (Young *et al.* 1995; Kenney & Young 1988), and the NRO 45 m telescope (Nishiyama 1995).

TABLE 2. Observed galaxies.

Galaxy	Type	Inclination† (deg)	P.A.† (deg)	Distance* (Mpc)	Linear Resd. (pc/15″)
NGC 598 (M33)	Sc	54	23(Obs:54)	0.79	55.3
NGC 1003	Scd	66	97	9.52	692
NGC 2403	Sc	60	127	3.32	241
UGC 2855	SBc	61	105	28.77	2092
NGC 2903	Sc	66	17	8.20	596
NGC 3034 (M82)	Ir	~90	80	3.25	236
NGC 3198	SBc	70	35	9.96	724
NGC 3521	Sbc	75	163	10.82	787
NGC 4096	Sc	73	20	12.22	889
NGC 4303	Sc	27	105(Obs:90)	11.17	498 × 310
NGC 4569	Sab	63	23(Obs:0)	10.65	510 × 250
NGC 4631	ScIr	84	86	4.30	313
NGC 5055	Sbc	55	105	9.82	714
NGC 5457(M101)	Sc	18	38	9.34	679
NGC 6674	SBb	55	143	42.62	3100
NGC 7331	Sbc	75	168	13.55	985

† Inclination and position angle are taken from the "Third Reference Catalogue of Bright Galaxies (RC3)" (de Vaucouleurs et al.,1991).

* The distances have been derived by applying the Tully-Fisher relation, as deseived in the text.

3. RESULTS

3.1 Position–Velocity Diagrams

The obtained data are presented in Fig. 1 in the form of position–velocity (PV) diagrams. We also show intensity profiles along the major axis and averaged velocity profiles, which have been obtained by averaging the PV diagrams in the velocity and position directions, respectively. Below, we describe individual galaxies. Velocities used in the description are corrected for the inclinations.

NGC 598 (M33): This nearby Sc galaxy is a member of the local group, showing diffuse, rather amorphous, spiral arms, and the bulge is small in size and luminosity. The PV diagram has been obtained along PA = 54°, about 30° different from the true PA at 23°. The CO emission is weak, and no rotating disk is visible in the central 30″ (110 pc). Therefore, no rotation curve was obtained for this galaxy.

NGC 1003: This is a tilted, two-armed spiral. The CO-line intensity is asymmetric with respect to the nucleus. The PV diagram indicates a steep rise of rotation near the nucleus in the negative velocity side, while the opposite side is only weakly detected. The gradient of rotation rise is as large as ~250 km s^{-1}/10″ (460 pc).

NGC 2403: This is an Sc galaxy with open spiral arms, morphologically similar to M33. The nuclear PV diagram shows a steep rise, reaching V_{rot}~170 km s^{-1} within the central 10″ (160 pc). Although the morphology is similar, the nuclear rotation is different from that for M33.

UGC 2855: This is an SBc type galaxy with high optical surface brightness, associated with a companion (UGC 2866) at a distance of 10′ (84 kpc) to the east. CO intensity as strong as T_A^*~0.45 K has been observed in the central part. The PV diagram shows a very steep rise to V_{rot} ~200 km s^{-1} within the central ~7″ (1 kpc), indicating a rapidly rotating disk. The negative velocity peak of this central disk attains a maximum velocity as high as

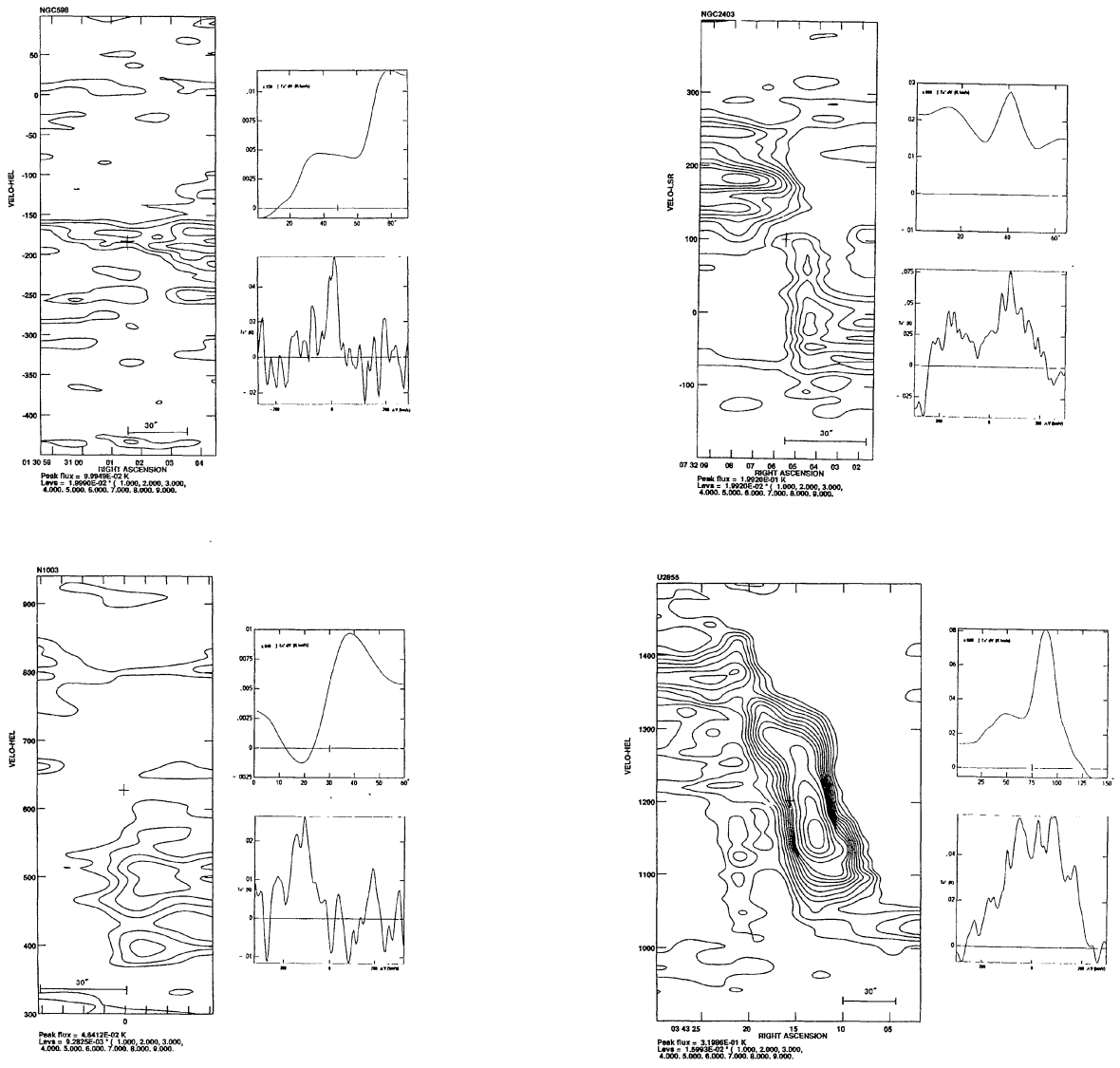

FIG. 1. Position–velocity (PV) diagrams in the CO ($J=2-1$) line emission along the major axes of nearby galaxies. The intensity scales are in T_a^* in K, and contour levels are indicated by the small tables. The left-upper panels show the distribution of CO intensity along the major axis, and the right-lower panels are averaged line profiles.

200 km s^{-1}/sin i=200 km s^{-1} within the central few arcseconds. Besides this steeply increasing component, the PV diagram indicates a rigid-body like ridge with a velocity gradient of 170 km s^{-1}/30″ (4 kpc), followed by a flat rotation part at 200 km s^{-1} at >30″.

NGC 2903: The PV diagram shows a steep rise within the central 7″ (280 pc) to $V_{\rm rot}$~160 km s^{-1}, and has a maximum at ~15″ (600 pc) at $V_{\rm rot}$~250 km s^{-1}. The main ridge of the PV diagram in the southern part has a peculiar step at 1′ (2.4 kpc) radius, with a flat part of about 170 km s^{-1} till 1′, and, then, steps up to a flat part at 200 km s^{-1}. The outer rotation from H I, however, is very flat until the edge.

NGC 3034 (M82): This peculiar edge-on galaxy has been extensively studied in the CO line. The rotation curve is known for its steep rise near the center, and is declining in a Keplerian fashion, suggesting a truncated outer mass by a close encounter with the parent massive galaxy, M81 (Sofue *et al.* 1992). Our data show the nuclear rise and high-density gaseous torus rotating at about 120 km s^{-1}, consistent with the earlier observations. We show this galaxy in order to demonstrate that the nuclear rise of rotation is common even to such a dwarf and peculiar galaxy as M82 in a high starburst activity.

NGC 3198: The PV diagram appears to consist of two components: a steeply rising ridge, attaining a high-velocity peak within 20″, and a rigidly rising component with a milder slope. The first rotation peak of V~170 km s^{-1} occurs at r=23″ (1100 pc). The rigid-body component has a gradient of 110 km s^{-1} in 30″ (1.4 kpc), probably due to a ring or arms of a radius of about 30″.

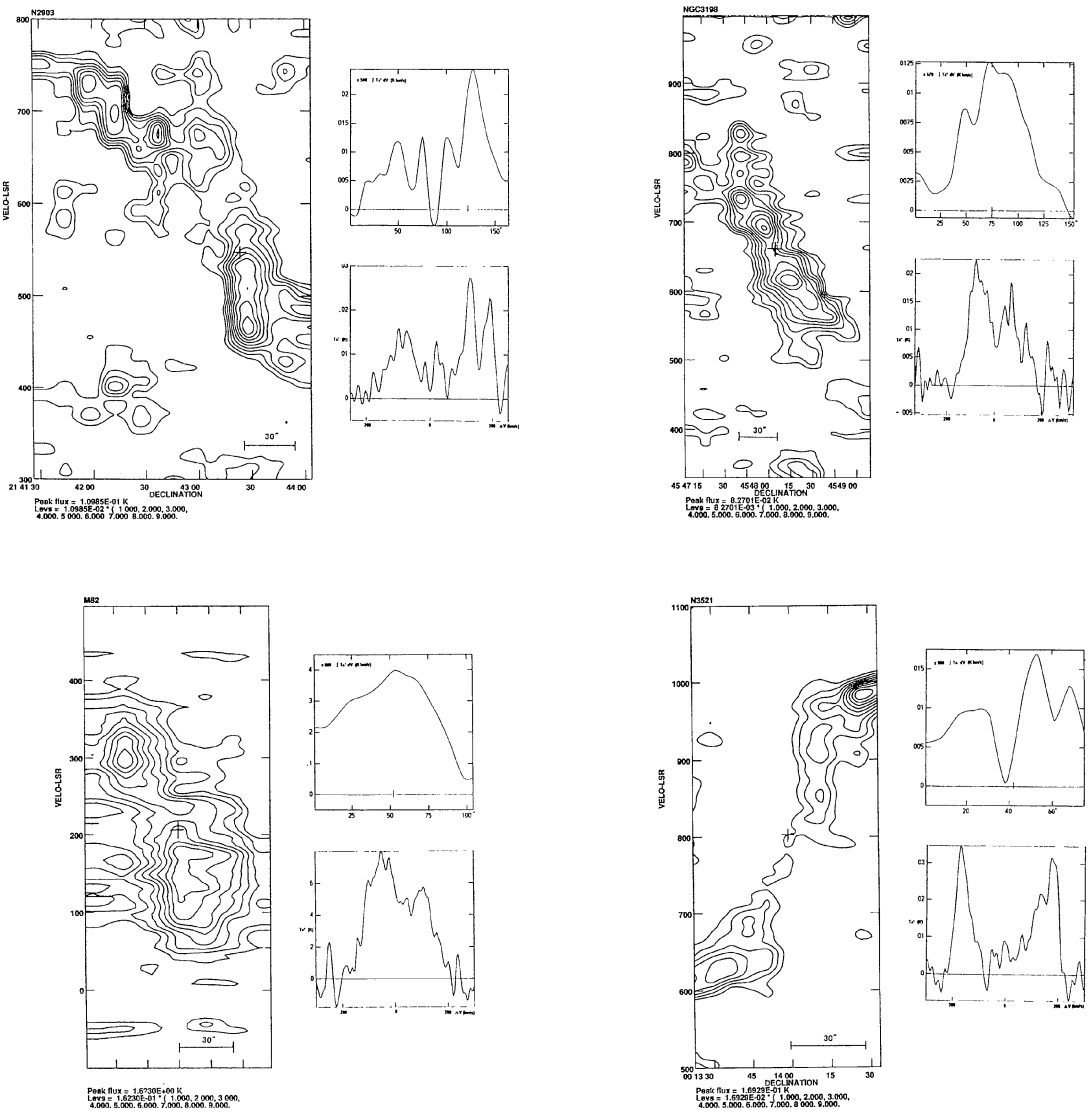

FIG. 1. (continued)

NGC 3521: The inner rotation velocity increases steeply, and attains a small and sharp central peak at 10″ (520 pc) of 210 km s^{-1}, followed by a dip at 20″ (1 kpc). It then increases slowly until a broad maximum at 1′.5 (4.7 kpc). However, the very center shows very weak emission, indicating either little CO gas in the center, or a very high velocity dispersion. The outer H I RC gradually decreases until the edge.

NGC 4096: This is an Sc galaxy with north-south asymmetry in the optical brightness distribution. The central CO distribution is also asymmetric, with the northern half stronger than the south. The PV diagram indicates a rotating ring of radius ~20″ with a rotating velocity of V_i~85 km s^{-1}. The CO rotation is followed by a flat part at a velocity of ~185 km s^{-1}. The nuclear few arcsec region shows no significant CO emission.

NGC 4303: This is a nearly face-on galaxy of Sc type, having a sign of bar. The CO intensity sharply peaks near the nucleus, and shows a high concentration within a radius of 15″ (0.8 kpc). The rotation velocity increases very steeply within 0.5 kpc to about 120 km s^{-1}.

NGC 4569: This Sab type galaxy shows also a high concentration of CO intensity near the center. The velocity increases very sharply within the central 5″ (300 pc) to about 200 km s^{-1}.

NGC 4631: This is an almost edge-on amorphous Sc galaxy, rich in CO gas. The rotation velocity increases in a rigid-body fashion, as slowly as ~100 km s^{-1}/1 kpc. This galaxy is one of the exceptions, which show rigid-body rotation.

NGC 5055: The PV diagram shows a very steep rise within ~6″ (210 pc) to a velocity of V_i~200 km s^{-1}. Then, the rotation velocity is almost constant till ±40″ (1.4 kpc).

NGC 5457 (M101): This is a nearly face-on Sc galaxy with i~18°. CO emission has been detected near the systemic velocity (241 km s^{-1}), with a velocity width of

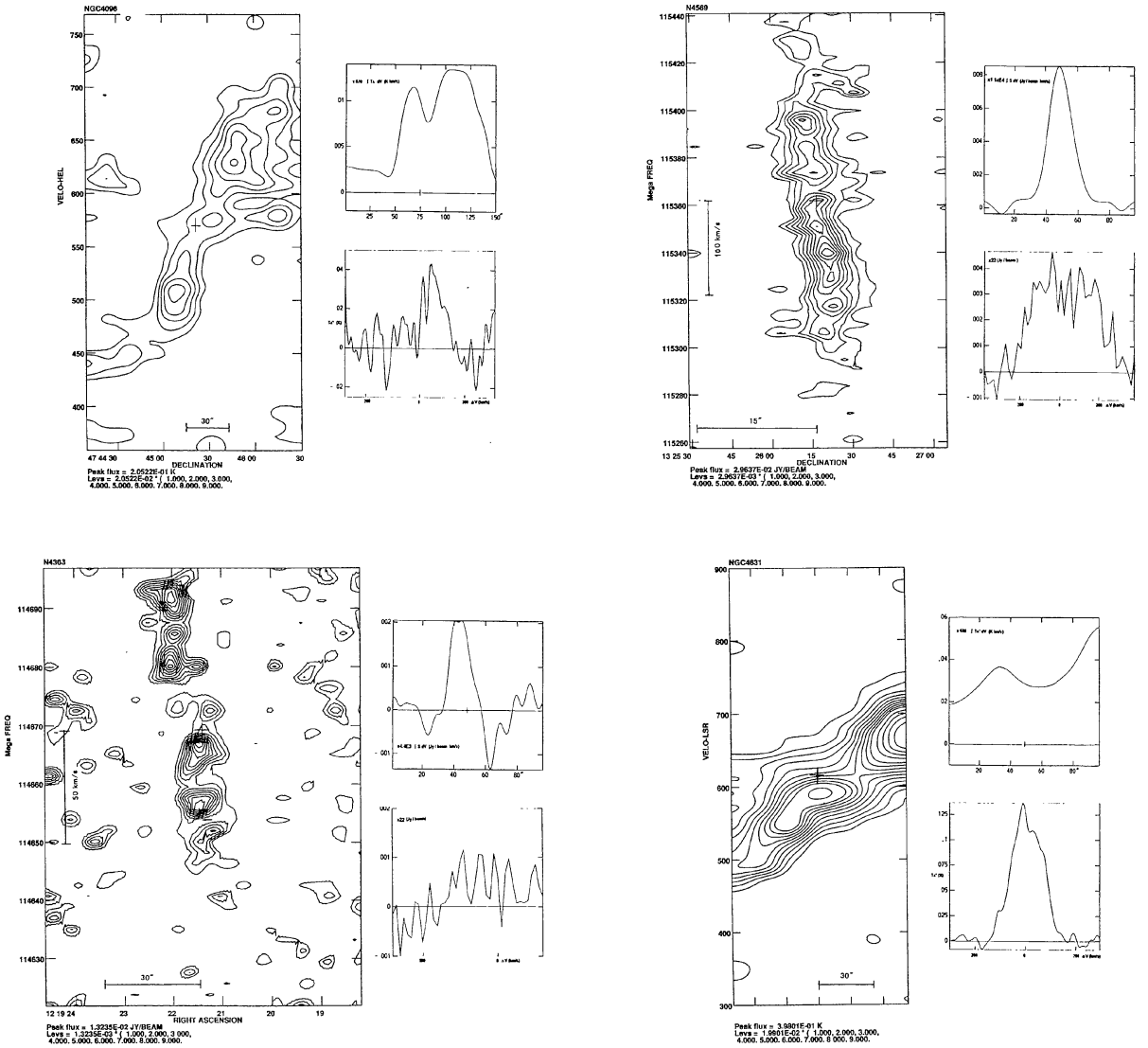

FIG. 1. (continued)

~ 70 km s^{-1}, which corresponds to 230 km s^{-1} within the disk plane. The northern half shows stronger emission with a negative velocity, while the southern half is not clearly detected. However, if two weak emission peaks in the north at $V_{\rm hel}\sim 170$ km s^{-1} and in the south at $V_{\rm hel}\sim 350$ km s^{-1} are due to the rotation, the rotation velocity is estimated to be as high as ~ 290 km s^{-1} within the central $\sim 10''$ (350 pc). For the poor data and low inclination, no rotation curve has been obtained.

NGC 6647: This is a bar-ringed galaxy, and weak CO emission has been detected. The obtained PV diagram is not of high-quality, but can be used to trace rotation velocities, indicating a steep rise of rotation up to 250 km s^{-1} within a few hundred pc of the center.

NGC 7331: The PV diagram shows a rigid-body increase, corresponding to a ring-like distribution of gas at a radius $30''$ (2 kpc) rotating at $V_{\rm rot}=250$ km s^{-1}. The rotation is then flat to $\pm 2'$ (8 kpc). The central $20''$ (1.4 kpc) region shows weak CO emission. The averaged velocity profile shows a typical double-horn property, characteristic to a rotation disk with a constant velocity.

3.2 Nuclear Rotation Curves

We adopt the envelope-tracing method (Sofue 1996) to derive rotation curves, which uses the loci of terminal velocity in position–velocity (PV) diagrams. We define the terminal velocity by a velocity at which the intensity becomes equal to

$$I_t=[(0.2I_{\rm max})^2+I_{\rm lc}^2]^{1/2} \quad (1)$$

on the PV diagrams. Here, $I_{\rm max}$ and $I_{\rm lc}$ are the maximum intensity and intensity corresponding to the lowest contour level, respectively. This equation defines a 20% level of the

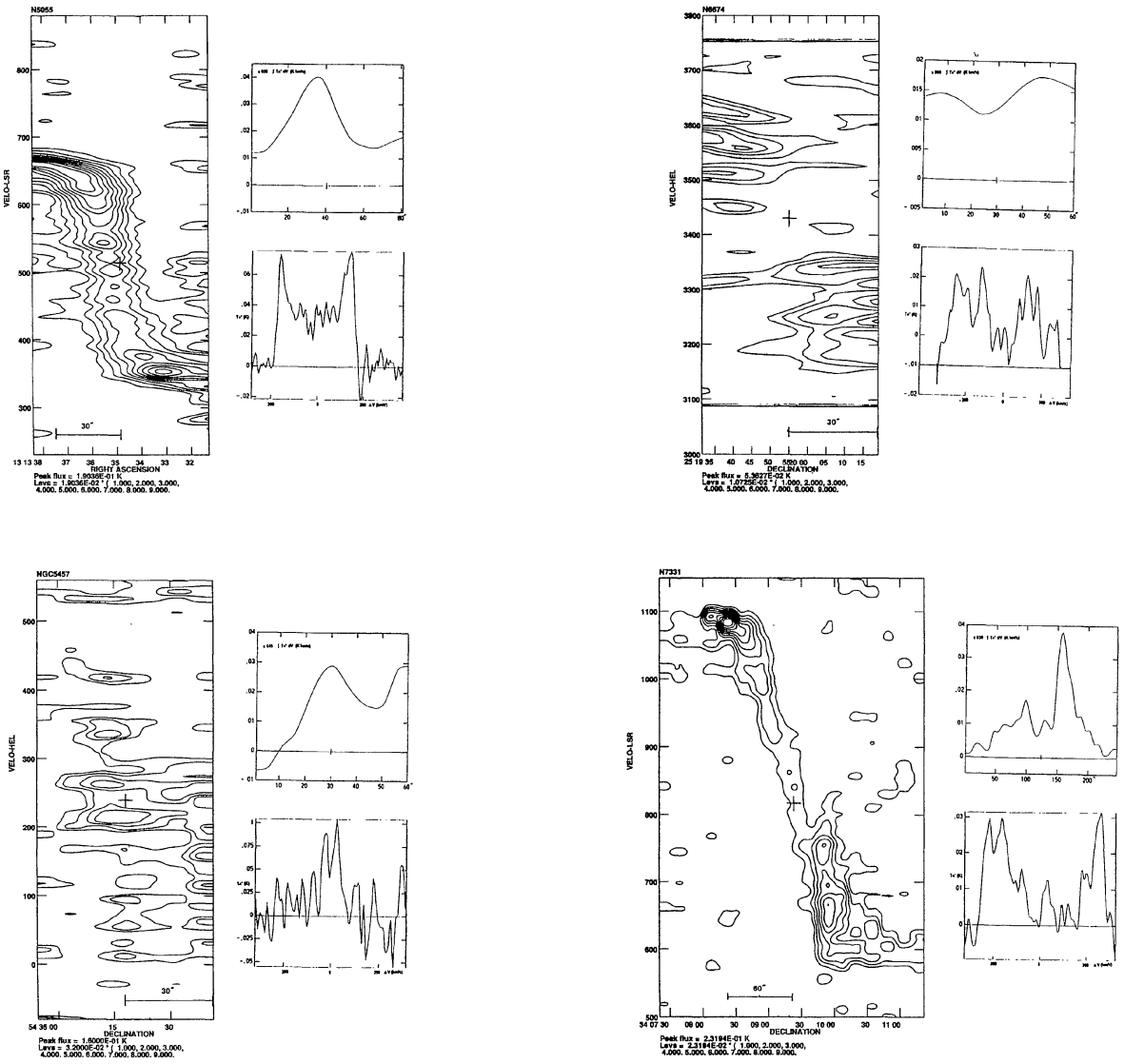

FIG. 1. (continued)

intensity profile at a fixed position, $I_t \simeq 0.2 \times I_{\max}$, if the signal-to-noise ratio is sufficiently high. If the intensity is not high enough, the equation gives $I_t \simeq I_{\rm lc}$, which approximately defines the loci along the lowest contour level ($\sim 3 \times$rms noise). The terminal velocity is then corrected for the velocity dispersion of the interstellar gas ($\sigma_{\rm ISM}$) and the velocity resolution of observations ($\sigma_{\rm obs}$) as

$$V_t^0 = V_t - (\sigma_{\rm obs}^2 + \sigma_{\rm ISM}^2)^{1/2}. \quad (2)$$

Small-scale structures due to clumpy ISM and clouds, and partly due to noise in the observations, are smoothed by eye estimates. The asymmetry with respect to the center of the PV diagram has been often observed. In such a case with asymmetry, we have averaged the measured velocities in both sides of the nucleus.

The rotation velocity is finally obtained by

$$V_{\rm rot} = V_t^0 / \sin i, \quad (3)$$

where i is the inclination angle of the disk plane. The accuracy of determining the terminal velocity, and therefore the accuracy of the obtained rotation curve, is typically $\pm 10/\sin i$ km s^{-1}. However, in some cases the rotation curves in both sides of the nucleus were not symmetric, and we have averaged the values in both sides. This often caused errors amounting to 15 to 20 km s^{-1}, larger than the error in the tracing of PV diagram itself.

Figure 2 shows the thus obtained rotation curves corrected for the inclination for 14 galaxies, for which PV diagrams with sufficient signal-to-noise ratio have been obtained. Figure 3 shows all curves plotted in the same scales both in radius and velocity. The horizontal and vertical bars of a cross attached to each curve indicate the FWHM of the telescope beam (linear length corresponding to 15″) and the

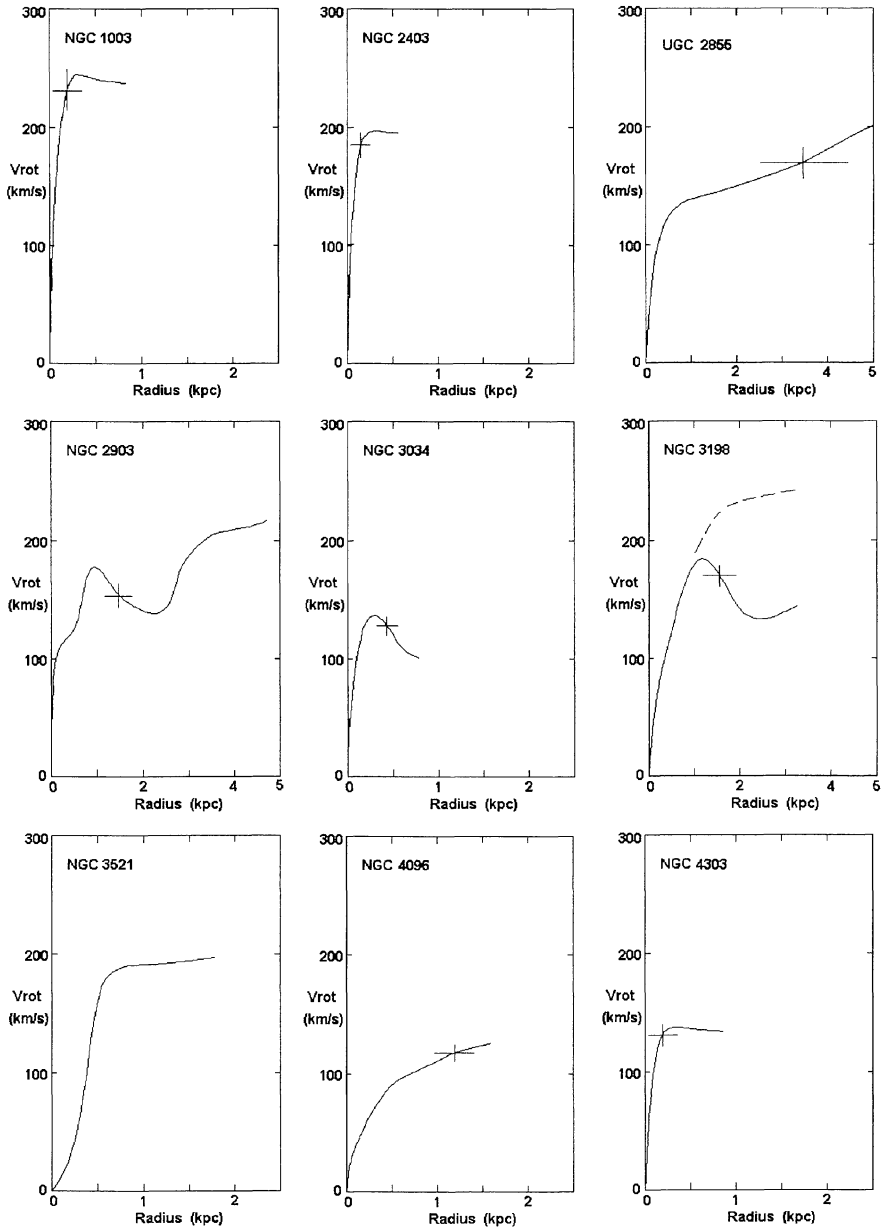

FIG. 2. Nuclear rotation curves for 14 galaxies, as derived by using the CO-line PV diagrams in Fig. 1. The velocities have been corrected for inclination, and the radii have been calculated corresponding to the distances given in Table 1. Typical errors in velocity (vertical bar) and resolution (horizontal bar) are given by the crosses attached to individual curves.

typical velocity error as described above, respectively. The radial distances were calculated by using the distances listed in Table 1, which were estimated by applying the B-band Tully–Fisher relation (Pierce & Tully 1992) using the data from the Reference Catalogue of Bright Galaxies (RC3; de Vaucouleurs *et al.* 1991):

$$M_B^{b,i} = -7.48(\log W_{i\,20} - 2.50) - 19.55.$$

Here, $W_{i\,20}$ and $M_B^{b,i}$ are, respectively, the H I linewidth measured at 20% level and B-band total absolute magnitude corrected for Galactic and internal extinction and for redshift taken from RC3.

4. DISCUSSION

4.1 Distribution of Molecular Gas

The intensity distribution of the CO-line emission along the major axis for the observed galaxies show more or less an asymmetry with respect to the nuclei. Such positional asymmetry and displacement of the CO intensity has been also observed in the Milky Way (e.g., Bally *et al.* 1987), and therefore, may be a common phenomenon in the central molecular disks of spiral galaxies.

However, if we adopt the kinematical centers of the observed CO PV diagrams, the rotation velocities, as defined

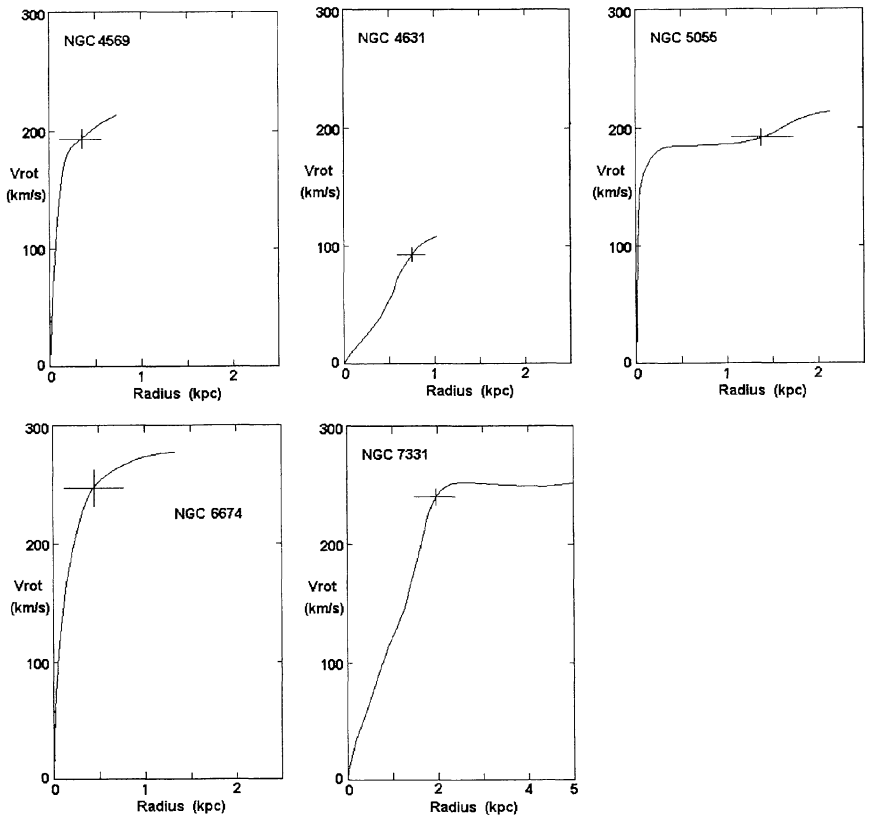

FIG. 2. (continued)

by the envelope-tracing method, are symmetric, in spite of the significant asymmetry of the intensity. This would be reasonable, if the mass of molecular gas is not large to affect the background gravitational potential of the inner disk and bulge of the galaxy. This is consistent with the fact that the mass fraction of the molecular gas within a few hundred pc of a galaxy is only several percent of the dynamical mass (Sofue 1995), if we adopt the new conversion factor which is a strong function of the metallicity (Arimoto *et al.* 1996).

4.2 Steep Rise of Rotation Curve

Figures 2 and 3 show that the rotation curves generally rise steeply within a radius smaller than the beam width of the CO observations, typically within a few hundred parsecs. This agrees with our earlier study of other galaxies (Sofue 1996, 1997), and with the recent Hα study of nuclear rotating disks in Virgo-cluster galaxies (Rubin *et al.* 1997). Although the central rising parts for some galaxies mimic rigid rotation, they may be mostly due to a lack of resolution. An exception is NGC 4631: In spite of the sufficient resolution, this galaxy shows a gradually rising rotation in a rigid-body fashion. NGC 7331 may be another case which shows an apparent rigid-body rise, while the CO emission of the very central region is too weak to prove this property. Such an apparently rigid-body behavior of PV diagram is often caused by a lack of molecular gas in the central region: A molecular ring in a highly-tilted galaxy would result in a rigid-body-like ridge on a PV diagram. Therefore, we may conclude that the steep rise, usually within a radius not resolved by the observing beam, is a general characteristics of rotation in the central regions of the observed galaxies.

In Papers I and II, we have shown that the steeply rising rotation curves can be fitted by a model with a mass distribution with a high central concentration, higher than that corresponding to the normal bulge component (Sofue 1996). Particularly, such a steep rise within the central 100 parsecs as obtained by high-resolution interferometer observations

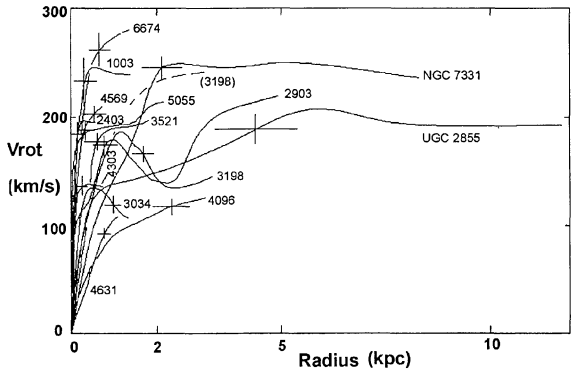

FIG. 3. The same as Fig. 2, but all curves are plotted in the same linear and velocity scales.

(e.g., NGC 4303, NGC 4569) indicates the existence of a compact nuclear mass of a 100–150 pc radius and a mass of several $10^9\ M_\odot$. Since the mass within the central 100 pc region is dominated by that of the bulge, such mass concentration may be deeply coupled with the dynamical structure and evolution of the central bulges. A detailed deconvolution of the rotation curves and comparison with optical and infrared surface photometry will be given in a separate paper.

4.3 Small Effect of a Bar?

If the molecular gas is in a noncircular motion such as due to a bar, it is not straightforward to use them to derive the mass. In Papers I and II, we have shown that the probability of looking at a bar parrallely is much smaller compared to that of looking at it perpendicularly or at a large angle, and therefore, such non-circular motion, if it is dominant, would result in a more number of galaxies showing rigid-body rotation than those showing a steep rise. However, our study, together with those in Papers I and II, shows that most galaxies have a steep nuclear rise. This fact indicates that the molecular gas is more likely to be rotating circularly, than to be in a bar-shocked non-circular motion. We finally mention that the mass distribution derived by assuming circular rotation have shown a good agreement with their surface photometry at radii of 1–5 kpc (e.g., Kent 1987), where the effect of bars would be most efficient.

The authors thank the staff of Nobeyama Radio Observatory for their help during the observations. This work has been performed as a common-use program of NRO.

REFERENCES

Clemens, D. P. 1985, ApJ, 295, 422
de Vaucouleurs, G., *et al.* 1991, Third Reference Catalogue of Bright Galaxies (Springer, New York)
Honma, M., Sofue, Y., & Arimoto, N. 1995, A&A, 304, 1
Kenney, J., & Young, S. J. 1988, ApJS, 66, 261
Kent, S. M. 1987, AJ, 93, 816
Nishiyama, K. 1995, Ph.D. thesis, University of Tokyo
Pierce, M. J., & Tully, R. B. 1992, ApJ, 387, 47
Rubin, V. C., Ford, W. K., & Thonnard, N. 1980, ApJ, 238, 471
Rubin, V. C., Ford, W. K., & Thonnard, N. 1982, ApJ, 261, 439
Rubin, V. C., Kenney, J. D. P., & Young, J. S. 1997, AJ, 113, 4
Sofue, Y. 1995, PASJ, 47, 527
Sofue, Y. 1996, ApJ, 458, 120 (Paper I)
Sofue, Y. 1997, PASJ, 49, 17 (Paper II)
Sofue, Y., Honma, M., & Arimoto, N. 1994, A&A, 296, 33
Sofue, Y., Reuter, H.-P., Krause, M., Wielebinski, R., & Nakai, N. 1992, ApJ, 395, 126
Young, J. S., *et al.* 1995, ApJS, 98, 219